Ghost imaging for an axially moving target with an unknown constant speed

Xiaohui Li, Chenjin Deng, Mingliang Chen, Wenlin Gong,* and Shensheng Han

Key Laboratory for Quantum Optics and Center for Cold Atom Physics, Shanghai Institute of Optics and Fine Mechanics, Chinese Academy of Sciences, Shanghai 201800, China
**Corresponding author: gongwl@siom.ac.cn*

Received March 25, 2015; revised April 29, 2015; accepted April 29, 2015; posted May 5, 2015 (Doc. ID 236857); published June 12, 2015

The influence of the axial relative motion between the target and the source on ghost imaging (GI) is investigated. Both the analytical and experimental results show that the transverse resolution of GI is reduced as the deviation of the target's center position from the optical axis or the axial motion range increases. To overcome the motion blur, we propose a deblurring method based on speckle-resizing and speed retrieval, and we experimentally validate its effectiveness for an axially moving target with an unknown constant speed. The results demonstrated here will be very useful to forward-looking GI remote sensing. © 2015 Chinese Laser Press

OCIS codes: (110.2990) Image formation theory; (270.0270) Quantum optics; (110.1758) Computational imaging; (100.2960) Image analysis.
http://dx.doi.org/10.1364/PRJ.3.000153

1. INTRODUCTION

Ghost imaging (GI), as a nonlocal imaging method, has theoretically and experimentally demonstrated that an unknown target can be reconstructed without scanning the target, when a single-pixel bucket detector is used to receive the target's transmitted (or reflected) signals [1–10]. This technique quickly aroused enormous interest in remote sensing, and factors affecting the imaging quality of GI, such as scattering and turbulence, have been widely investigated [11–20]. Recently, super-resolution GI, three-dimensional GI lidar, and full-color GI can also be achieved [20–23]. However, all previous works on GI have been concerned with static targets [11–22]. In practical applications of remote sensing, imaging an unstable or moving target is much more meaningful because there is usually relative motion between the imaging system and the target.

There are two cases of relative motion between the imaging system and the target. One is in the tangential direction, and the other is in the axial direction. For the former, some theoretical and experimental results have shown that the tangential relative motion between the GI system and the target will cause the degradation of transverse resolution [24,25]. Based on the character of GI, some methods are invented to overcome the motion blur [26,27]. For the latter and its correspondence to forward-looking imaging in practice, there is no relevant discussion at present. According to the analytical results described in [7], the magnification of recovered images will vary with the axial distance between the source plane and the target plane when the reference path of the GI system is fixed. Therefore, the axial relative motion between the GI system and the target will also lead to the degradation of transverse resolution. In this work, the influence of axial motion on GI is investigated both theoretically and experimentally. To overcome the motion blur, a deblurring method for an axial moving target with an unknown constant speed is invented and its effectiveness is experimentally validated.

2. ANALYTICAL RESULTS

Figure 1 shows the experimental schematic of lensless pseudo-thermal light GI for an axially moving target. The pseudo-thermal light is obtained by passing a laser beam through a slowly rotating ground glass disk (the wavelength $\lambda = 532$ nm, and the light spot's transverse size $D = 2$ mm on the rotating ground glass disk plane). By using a beam splitter, the light is divided into a test and a reference path. In the reference path, the light propagates directly to a charge-coupled device (CCD) camera D_r. In the test path, the intensity transmitted through the target is collected by a lens f onto a single-pixel bucket detector D_t. The target is placed on a motion platform, and the platform is driven by a stepping motor; thus it can move along the optical axis. In addition, the stepping accuracy of the platform is 1 μm, and the stepping motor is connected to a computer, which can control the target's motion.

For GI [1,2], the second-order correlation function of intensity fluctuations between two detectors is

$$\Delta G^{(2,2)}(x_r, x_t) = \left| \int \mathrm{d}x_1 \int \mathrm{d}x_2 G^{(1,1)}(x_1, x_2) h_r^*(x_r, x_1) h_t(x_t, x_2) \right|^2, \tag{1}$$

where $G^{(1,1)}(x_1, x_2)$ is the first-order correlation function of the light field on the rotating ground glass plane. x_1 and x_2 are the coordinates on the source plane. $h_t(x_t, x_2)$ is the impulse response function of the test path, and $h_r^*(x_r, x_1)$ denotes the phase conjugate of the impulse response function in the reference path. In addition, x_r is the coordinate on the CCD camera plane, and x_t is the coordinate on the detector D_t plane.

For the schematic shown in Fig. 1, under the paraxial approximation, the impulse response function of the reference path is

$$h_r(x_r, x_1) \propto \exp\left\{ \frac{j\pi}{\lambda z} (x_r - x_1)^2 \right\}, \tag{2}$$

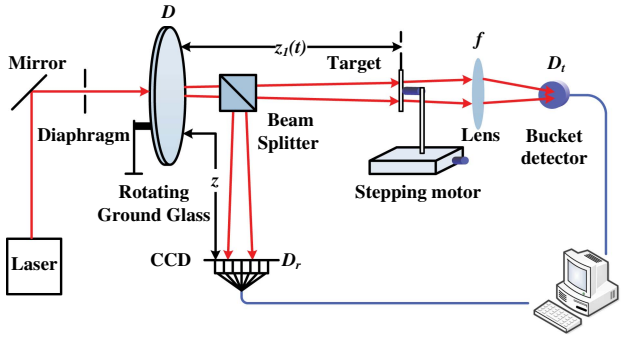

Fig. 1. Experimental schematic of lensless pseudo-thermal light GI for an axially moving target.

where z denotes the distance between the source plane and the CCD camera plane.

When the target moves along the optical axis with an unknown constant speed v_0, the distance between the source plane and the object plane is time-dependent, namely $z_1(t) = z_0 + v_0 t$. Thus the impulse response function for the test path at time t can be expressed as

$$h_t(x_t, x_2) \propto \int \mathrm{d}x \, \exp\left\{\frac{j\pi}{\lambda z_1(t)}(x_2 - x)^2\right\} t(x) h_t(x_t, x), \tag{3}$$

where $t(x)$ is the target's transmission function and x is the coordinate on the object plane, and $h_t(x_t, x)$ is the impulse response function from the target plane to the detector D_t.

For pseudo-thermal light GI, the intensity distribution modulated by the rotating ground glass disk follows a negative exponential distribution function [28]. If the source is large enough relative to the object, the light field generated by the rotating ground glass disk can be considered to be fully spatially incoherent, and the intensity distribution can be assumed to be uniform as a constant intensity I_0, then

$$G^{(1,1)}(x_1, x_2) = I_0 \delta(x_1 - x_2), \tag{4}$$

where $\delta(x)$ is the Dirac delta function.

Substituting Eqs. (2)–(4) into Eq. (1), the correlation function of intensity fluctuations is

$$\Delta G^{(2,2)}(x_r, x_t) \propto \left| \int \mathrm{d}x \int \mathrm{d}x_2 t(x) \exp\left(\frac{j\pi}{\lambda z_1(t)} x^2\right) \times h_t(x_t, x) \exp\left[\frac{j\pi}{\lambda}\left(\frac{1}{z_1(t)} - \frac{1}{z}\right) x_2^2\right] \times \exp\left[\frac{j2\pi}{\lambda}\left(\frac{x_r}{z} - \frac{x}{z_1(t)}\right) x_2\right] \right|^2. \tag{5}$$

When the target's axial motion is restricted in the range of axial correlation depth of light field (ACDF) described in [29], namely $\Delta z = |z - z_1(t)| < 6.7\lambda(z/D)^2$ for a circular-shaped source, then the quadratic term including x_2 in Eq. (5) is approximately a constant (namely, $\exp\{j\pi[1/z_1(t) - 1/z] x_2^2/\lambda\} \approx 1$). After calculating the integral of x_2, Eq. (5) can be rewritten as

$$\Delta G^{(2,2)}(x_r, x_t) \propto \left| \int \mathrm{d}x t(x) \exp\left(\frac{j\pi}{\lambda z_1(t)} x^2\right) \times h_t(x_t, x) \mathrm{sinc}\left[\frac{D}{\lambda}\left(\frac{x_r}{z} - \frac{x}{z_1(t)}\right)\right] \right|^2, \tag{6}$$

where $\mathrm{sinc}(x) = \sin(\pi x)/\pi x$, and D denotes the transverse size of the source. Since the bucket detector D_t collects all intensity information from the object, we can obtain

$$\Delta G^{(2,2)}(x_r) = \int \mathrm{d}x_t \Delta G^{(2,2)}(x_r, x_t) \propto \int \mathrm{d}x |t(x)|^2 \, \mathrm{sinc}^2\left\{\frac{D}{\lambda z}[x_r - M(t)x]\right\}, \tag{7}$$

where $M(t) = z/z_1(t)$ is the imaging magnification. From Eq. (7), it is observed that the magnification of recovered images will vary with the distance z_1 when the camera D_r in the reference path of the GI system is fixed.

According to the Klyshko's picture [30], Fig. 2 illustrates the explanation of motion blur of lensless pseudo-thermal light GI for an axially moving target shown in Fig. 1. The target's motion range, noted as $[z_{1\,\min}, z_{1\,\max}]$, is constrained in the ACDF of the target plane located at $z_1(t) = z$ from the source. By the reversibility of the light field, as shown in Fig. 2, the target is illuminated by a light source emitting the light from the bucket detector D_t and then is reflected by the phase conjugated mirror S to the CCD camera D_r. When the distance between the source plane S and the target plane $z_1(t)$ varies, an image with the magnification $M(t) = z/z_1(t)$ can be achieved on the CCD camera D_r. Therefore, for the image deviated from the optical axis Δx on the target's plane, when the CCD camera D_r in the reference path is fixed and the target's motion range is restricted in $[z_{1\,\min}, z_{1\,\max}]$, as illustrated in Fig. 2, the corresponding GI will move along the axis x_r of the CCD camera D_r plane with the increase of $z_1(t)$, and the motion blur on the camera D_r plane is $\Delta x_r = (z/z_{1\,\min} - z/z_{1\,\max})\Delta x \simeq \Delta z_1 \Delta x / z$ (where $\Delta z_1 = z_{1\,\max} - z_{1\,\min}$). The results imply that the target's transverse imaging resolution will decrease with an increase of the deviation of the target's center position from the optical axis Δx or Δz_1.

In order to overcome the motion blur problem of GI for an axially moving target with an unknown constant speed, we propose a deblurring method based on speckle-resizing and speed retrieval. According to the property of ACDF, the speckle located in the range of ACDF is similar, and only the magnification is different. Therefore, when the target is moving from $z_{1\,\min}$ to $z_{1\,\max}$ with a constant speed v_0, we can resize the speckle via the magnification $1/M(t)$ based on the speckle distribution recorded by the CCD camera D_r. By

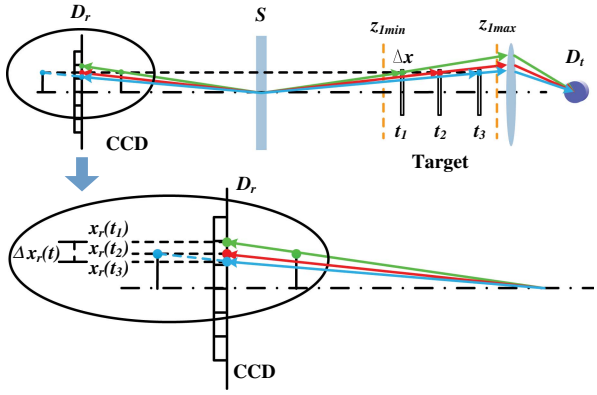

Fig. 2. Phenomenological explanation of motion blur of lensless pseudo-thermal light GI for an axially moving target. The pseudo-thermal light S acts as a phase conjugated mirror.

calculating the intensity correlation function between the resized speckle distributions and the intensities recorded by the bucket detector D_t, a deblurred image can be reconstructed. In practice, the moving speed of the target is unknown; thus the estimated accuracy to the speed v_0 directly affects the imaging resolution of the retrieved image. In order to determine the speed v_0, we can calculate the discrepancy $D(v)$ between the estimated signal $B_s^v, (s = 1, 2, 3, \ldots, K)$ and the signal $B_s, (s = 1, 2, 3, \ldots, K)$ directly recorded by the bucket detector, namely

$$D(v) = \frac{\sum_{s=1}^{K} [B_s - B_s^v]^2}{\sum_{s=1}^{K} B_s^2}, \tag{8}$$

where $B_s^v = \int \mathrm{d}x I_s^v(x)|t^v(x)|^2, \forall_s = 1 \ldots K$. In addition, $I_s^v(x)$ is the intensity distribution of the resized speckle, and $t^v(x)$ denotes the corresponding reconstructed image at the estimated speed v. Theoretically, when $D(v) = 0$, the estimated speed v is equal to v_0, which determines the target's accurate moving speed. In practice, because the measurement number K is finite and the detection noise is inevitable, we confirm that the target's moving speed is corresponding to the case of the minimum value of $D(v)$. Further, only when the moving speed is properly estimated can the image $t^v(x)$ without motion blur be achieved. Therefore, by searching over the estimated speed space and identifying the minimum value of $D(v)$, one can not only determine the motion speed of a target but also overcome the influence of axial motion on the imaging resolution of GI for a moving target with a constant speed.

3. EXPERIMENTAL RESULTS

To verify the above concept and analytical results, we carried out experimental tests with a double slit (slit width $a = 110$ μm, slit height $h = 900$ μm, and center-to-center separation $d = 260$ μm) in different motion conditions, using the lensless pseudo-thermal light GI scheme depicted in Fig. 1. The distance between the CCD camera D_r and the source plane is fixed as $z = 400$ mm. The exposure time window for both the camera D_r and the detector D_t is set to be 1 ms, and the sampling frequency is 10 Hz. The transverse size of the speckle on the CCD camera is about 106 μm, and the measurement number is $K = 5000$. Figure 3(a) present the experimental demonstration results of the influence of the deviation Δx on GI for an axially moving target with a constant speed. In this case, the start line of the motion is set as $z_{1\,\mathrm{min}} = 380$ mm, and the motion speed is about $v_0 = 80$ μm/s; then $\Delta z_1 \simeq 40$ mm. In Fig. 3(a), we show the reconstruction results of GI without speckle-resizing when the target's center position is located at $\Delta x = 0$, 1.0, 2.0, 3.0, 4.0, and 5.0 mm, respectively. According to $\Delta x_r \simeq \Delta z_1 \Delta x / z$, the corresponding motion blur in the x_r direction of the camera D_r plane is 0, 0.1, 0.2, 0.3, 0.4, and 0.5 mm, respectively. Therefore, as displayed in Fig. 3(a), it is clearly seen that the transverse resolution of GI in the x_r direction reduces with the increase of Δx, which is in accordance with the analytical results. Similarly, $\Delta y_r \simeq \Delta z_1 \Delta y / z$, and the maximum value of Δy is 450 μm for the double-slit (half of the slit height), thus the largest motion blur in y_r direction is 45 μm, which is less than the speckle's transverse size on the CCD camera plane and the transverse resolution in y_r direction hardly degrades. By searching over the estimated speed space (the process takes about 30 s on a normal PC), the relationship between the discrepancy $D(v)$ and the speed v for the case of $\Delta x = 4.0$ mm is shown in Fig. 3(d). From the curve $D(v) - v$, the corresponding motion speed is 82 μm/s for the minimum value of $D(v)$ (namely the point C on the curve), which coincides with the true motion speed of the target. Relative to the results displayed in Fig. 3(a), Fig. 3(c) illustrates the corresponding deblurring reconstruction results when the motion speed is estimated as $v = 82$ μm/s. In order to compare with the results shown in Fig. 3(c), Fig. 3(b) gives the retrieved images with the speckle-resizing method when the motion speed is estimated as $v = 48$ μm/s [corresponding to the point B on the curve shown in Fig. 3(d)]. It is obviously observed that the motion blur can be removed only when the speed of the moving target is correctly estimated.

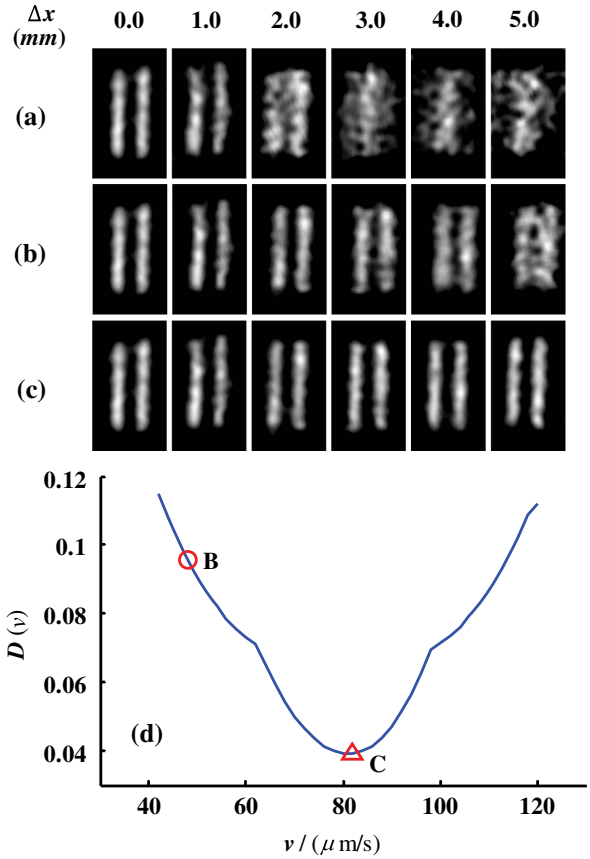

Fig. 3. Experimental reconstruction results of GI without and with speckle-resizing for an axially moving target with an unknown constant speed (the motion speed is about 80 μm/s and the axial motion range $\Delta z_1 = 40$ mm). (a) GI reconstruction result without speckle-resizing; (b) GI reconstruction results with speckle-resizing, corresponding to the estimated speed of point B (○) labeled in (d); (c) GI reconstruction results with speckle-resizing, corresponding to the estimated speed of point C (△) labeled in (d); (d) relationship between the discrepancy $D(v)$ and v (corresponding to the case $\Delta x = 4.0$ mm). From the left to right of (a) through (c), the deviation of the target's center position from the optical axis Δx is 0, 1.0, 2.0, 3.0, 4.0, and 5.0 mm.

When the deviation of the target's center position is fixed as $\Delta x = 4.0$ mm, Fig. 4 gives the experimental reconstruction results of GI without and with speckle-resizing in different motion ranges Δz_1, and the other conditions are the same as in Fig. 3. Based on the ACDF described in [29], the ACDF of the target plane located at $z_1(t) = z = 400$ mm is about

$\Delta z = 142$ mm. In Fig. 4(a), the start line of the motion is set as $z_{1\,\min} = 390$ mm, and the motion speed is about $v_0 = 40$ μm/s; thus $z_{1\,\max}$ is about 410 mm (namely $\Delta z_1 \simeq 20$ mm). In Fig. 4(b), $z_{1\,\min}$ is 380 mm and $z_{1\,\max}$ is about 420 mm (namely $\Delta z_1 \simeq 40$ mm). In Fig. 4(c), $z_{1\,\min}$ is 370 mm and $z_{1\,\max}$ is about 430 mm (namely $\Delta z_1 \simeq 60$ mm). Using the proposed speckle-resizing method based on speed retrieval and by searching over the estimated speed space, the corresponding motion speeds for Figs. 4(a)–4(c) are about 44, 82, and 120 μm/s, respectively. From the results shown in Figs. 4(a)–4(c), similar to the case demonstrated in Fig. 3, it is clearly seen that the imaging resolution of GI decreases with the increase of the motion range Δz_1, and the motion blur can also be overcome by our proposed deblurring method.

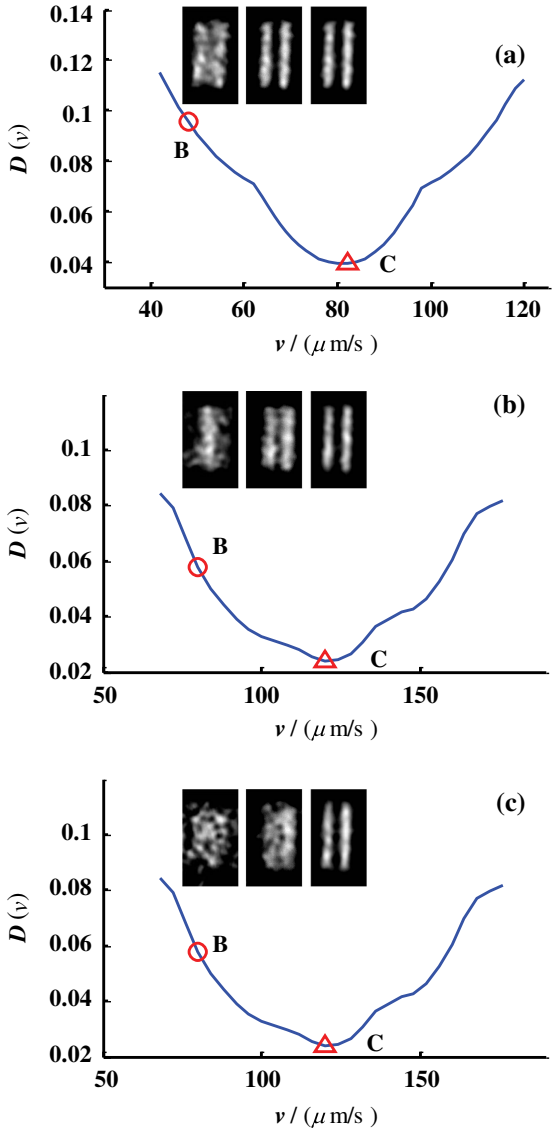

Fig. 4. Effect of the motion range Δz_1 on GI without and with speckle-resizing (the deviation of the target's center position Δx is fixed as 4.0 mm). (a) For small motion range, $\Delta z_1 = 20$ mm, the motion speed is approximately 40 μm/s; (b) for medium motion range, $\Delta z_1 = 40$ mm, the motion speed is approximately 80 μm/s; (c) for large motion range, $\Delta z_1 = 60$ mm, the motion speed is approximately 120 μm/s. For (a) through (c), the corresponding experimental reconstruction results of GI without and with speckle-resizing are listed at upper left corners: the left subfigure is the GI reconstruction result without speckle-resizing; the middle subfigure is the GI reconstruction results with speckle-resizing, corresponding to the estimated speed of point B (○); and the right subfigure is the GI reconstruction results with speckle-resizing, corresponding to the estimated speed of point C (△).

4. CONCLUSION

In conclusion, we have theoretically and experimentally demonstrated that the axial relative motion between the target and the source will result in the degradation of transverse resolution for GI. As the deviation of the target's center position from the optical axis Δx or the motion range Δz_1 increases, the imaging resolution will become worse. Using the proposed deblurring method based on speckle-resizing and speed retrieval, our experimental results indicate that the motion speed of the target can be determined and the degradation of imaging resolution caused by the motion blur can also be overcome. This method can be directly applied to forward-looking GI.

ACKNOWLEDGMENTS

The work was supported by the Hi-Tech Research and Development Program of China under Grant Project No. 2013AA122901.

REFERENCES

1. J. Cheng and S. Han, "Incoherent coincidence imaging and its applicability in X-ray diffraction," Phys. Rev. Lett. **92**, 093903 (2004).
2. A. Gatti, E. Brambilla, M. Bache, and L. A. Lugiato, "Ghost imaging with thermal light: comparing entanglement and classical correlation," Phys. Rev. Lett. **93**, 093602 (2004).
3. M. D'Angelo and Y. H. Shih, "Quantum imaging," Laser Phys. Lett. **2**, 567–596 (2005).
4. D. Z. Cao, J. Xiong, and K. Wang, "Geometrical optics in correlated imaging systems," Phys. Rev. A **71**, 013801 (2005).
5. D. Zhang, Y.-H. Zhai, L.-A. Wu, and X.-H. Chen, "Correlated two-photon imaging with true thermal light," Opt. Lett. **30**, 2354–2356 (2005).
6. A. Gatti, M. Bache, D. Magatti, E. Brambilla, F. Ferri, and L. A. Lugiato, "Coherent imaging with pseudo-thermal incoherent light," J. Mod. Opt. **53**, 739–760 (2006).
7. W. Gong, P. Zhang, X. Shen, and S. Han, "Ghost 'pinhole' imaging in Fraunhofer region," Appl. Phys. Lett. **95**, 071110 (2009).
8. Y. Bromberg, O. Katz, and Y. Silberberg, "Ghost imaging with a single detector," Phys. Rev. A **79**, 053840 (2009).
9. B. I. Erkmen and J. H. Shapiro, "Ghost imaging: from quantum to classical to computational," Adv. Opt. Photon. **2**, 405–450 (2010).
10. J. H. Shapiro and R. W. Boyd, "The physics of ghost imaging," Quantum Inf. Process. **11**, 949–993 (2012).
11. J. Cheng, "Ghost imaging through turbulent atmosphere," Opt. Express **17**, 7916–7921 (2009).
12. P. Zhang, W. Gong, X. Shen, and S. Han, "Correlated imaging through atmospheric turbulence," Phys. Rev. A **82**, 033817 (2010).
13. W. Gong and S. Han, "Correlated imaging in scattering media," Opt. Lett. **36**, 394–396 (2011).
14. N. D. Hardy and J. H. Shapiro, "Reflective ghost imaging through turbulence," Phys. Rev. A **84**, 063824 (2011).
15. R. E. Meyers, K. S. Deacon, and Y. Shih, "Turbulence-free ghost imaging," Appl. Phys. Lett. **98**, 111115 (2011).
16. C. Zhao, W. Gong, M. Chen, E. Li, H. Wang, W. Xu, and S. Han, "Ghost imaging lidar via sparsity constraints," Appl. Phys. Lett. **101**, 141123 (2012).
17. B. I. Erkmen, "Computational ghost imaging for remote sensing," J. Opt. Soc. Am. A **29**, 782–789 (2012).
18. M. Chen, E. Li, W. Gong, Z. Bo, X. Xu, C. Zhao, X. Shen, W. Xu, and S. Han, "Ghost imaging lidar via sparsity constraints in real atmosphere," Opt. Photon. J. **3**, 83–85 (2013).

19. N. D. Hardy and J. H. Shapiro, "Computational ghost imaging versus imaging laser radar for three-dimensional imaging," Phys. Rev. A **87**, 023820 (2013).
20. W. Gong, C. Zhao, J. Jiao, E. Li, M. Chen, H. Wang, W. Xu, and S. Han, "Three-dimensional ghost imaging ladar," arXiv:1301.5767 [Quant-ph].
21. W. Gong and S. Han, "Experimental investigation of the quality of lensless super-resolution ghost imaging via sparsity constraints," Phys. Lett. A **376**, 1519–1522 (2012).
22. W. Gong and S. Han, "High-resolution far-field ghost imaging via sparsity constraint," Sci. Rep. **5**, 9280 (2015).
23. S. S. Welsh, M. P. Edgar, R. Bowman, P. Jonathan, B. Sun, and M. J. Padgett, "Fast full-color computational imaging with single-pixel detectors," Opt. Express **21**, 23068–23074 (2013).
24. H. Li, J. Xiong, and G. Zeng, "Lensless ghost imaging for moving objects," Opt. Eng. **50**, 127005 (2011).
25. C. Zhang, W. Gong, and S. Han, "Ghost imaging for moving targets and its application in remote sensing," Chin. J. Lasers **39**, 1214003 (2012).
26. C. Zhang, W. Gong, and S. Han, "Improving imaging resolution of shaking targets by Fourier-transform ghost diffraction," Appl. Phys. Lett. **102**, 021111 (2013).
27. E. Li, Z. Bo, M. Chen, W. Gong, and S. Han, "Ghost imaging of a moving target with an unknown constant speed," Appl. Phys. Lett. **104**, 251120 (2014).
28. J. W. Goodman, *Speckle Phenomena in Optics: Theory and Applications* (Roberts and Company, 2005).
29. W. Gong and S. Han, "The influence of axial correlation depth of light field on lensless ghost imaging," J. Opt. Soc. Am. B **27**, 675–678 (2010).
30. D. N. Klyshko, *Photons and Nonlinear Optics* (Gordon and Breach, 1988).